

Part I Materials

1

Organic Semiconductor Materials for Transistors

David Ian James, Jeremy Smith, Martin Heeney, Thomas D. Anthopoulos, Alberto Salleo, and Iain McCulloch

1.1

General Considerations

Recent advances in the electrical performance of organic semiconductor materials position organic electronics as a viable alternative to technologies based on amorphous silicon (a-Si). Traditionally a-Si-based transistors, which are used as the switching and amplifying components in modern electronics [1], require energy intensive batch manufacturing techniques. These include material deposition and patterning using a number of high-vacuum and high-temperature processing steps in addition to several subtractive lithographic patterning and mask steps, limiting throughput. Although this allows for the cost of individual transistors to be extremely low because of the high circuit density that can be obtained, the actual cost per unit area is very high. Alternatively, organic semiconductors can be formulated into inks and processed using solution-based printing processes [2–5]. This allows for large-area, high-throughput, low-temperature fabrication of organic field-effect transistors (OFETs), enabling not only a reduction in cost but also the migration to flexible circuitry, as lower temperatures enable the use of plastic substrates. The potential applications for these OFETs are numerous, ranging from flexible backplanes in active matrix displays to item-level radiofrequency identification tags.

OFETs are typically p-type (hole transporting) devices that are composed of a source and drain electrode connected by an organic semiconductor, with a gate electrode, insulated from the organic semiconductor via a dielectric material, as shown in Figure 1.1b. Holes are injected into the highest occupied molecular orbital (HOMO) of the organic semiconductor upon application of a negative gate voltage. The holes migrate to the accumulation layer, which forms at the semiconductor interface with the dielectric, and are transported between the source and drain upon application of an electric field between the two. Modulation of the gate voltage is used to turn the transistor ON and OFF, with the ON current and voltage required to turn the device on being figures of merit for the electrical performance of the device. The performance of the transistor is also governed by the charge carrier mobility of the semiconductor, which should be high to ensure fast charging speeds.

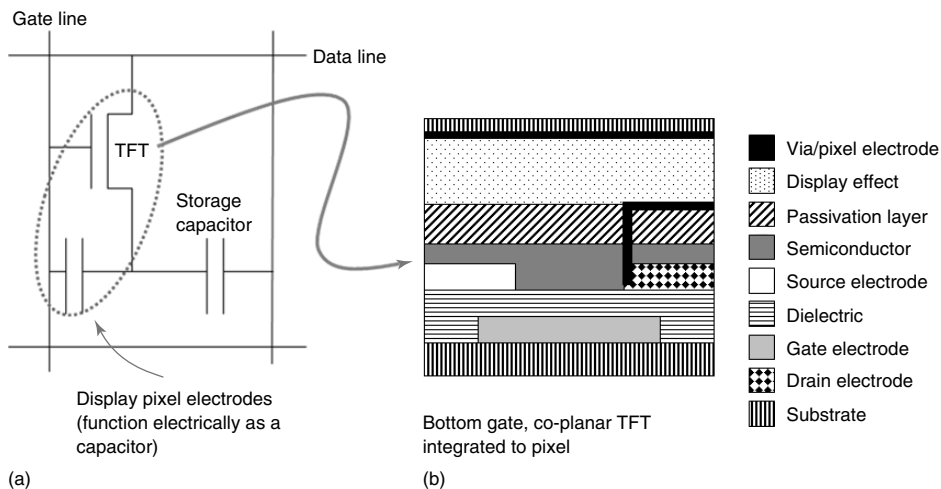


Figure 1.1 (a) Simple diagram of active matrix backplane circuitry and (b) cross section of corresponding TFT and pixel architecture.

In displays, OFETs can act as individual pixel switches in the backplane active matrix circuitry, as shown in Figure 1.1a. This technology is currently being used commercially in small-sized electrophoretic displays (EPDs), marketed as e-paper [6], to charge both the pixel and the storage capacitor. Active matrix backplanes are found in both liquid crystal displays (LCDs) and organic light emitting diode (OLED) displays, where a transistor also provides current to the emitting diode element. An advantage of the EPD effect is that the pixels are reflective to ambient light, which allows the pixel transistor to occupy the majority of the area underneath the pixel. This maximizes the transistor width, enabling more current to be delivered to the pixel, resulting in lower mobility specifications being required from the semiconductor. For small-sized devices ($\lesssim 10$ cm diagonally) with low resolutions and low refresh rates, the mobility required is in the region of $0.01 \text{ cm}^2 \text{ V}^{-1} \text{ s}^{-1}$, which is well within the capabilities of both polymer and small molecule semiconductors. In comparison, medium- to large-sized LCDs commonly used for monitor and television displays require semiconductor mobilities in excess of $0.5 \text{ cm}^2 \text{ V}^{-1} \text{ s}^{-1}$, and currently employ a-Si or polysilicon for higher-resolution displays. EPDs are also bistable, as once the pixel and the storage capacitor are charged, no additional power is needed to maintain the image. This minimizes the duty cycle load of the transistor, thus extending the lifetime. One problem with EPDs is that it is possible for ionic impurities within the liquid EPD cell to facilitate current leakage from the capacitor, which means that higher charge carrier mobilities are required than would be expected and thus high-purity electrophoretic inks are required to reduce the current demands of the display effect.

The function of the transistor in a LCD is to apply an electric field across the pixel, thus switching the direction of the optical axis of the liquid crystals,

which therefore generates the image. As the display operates in the transmissive mode, the transistor is directly in the path of the light source, and so must be small to maximize the aperture ratio of the pixel and thus increase the efficiency of light output. However, the use of smaller transistors means that the organic semiconducting material within the transistor needs to have a higher charge carrier mobility than that of the materials used in EPDs.

OLED displays have the potential to be fabricated using high-throughput printing techniques such as gravure or ink jet. Using organic transistors will allow for the complete integration of both front- and backplane fabrication processes. Top emitting devices, in which the OLED frontplane cathode is transparent, can be fabricated, allowing the OFET to be positioned underneath the emissive layer. Thus, the OFETs can be larger per pixel than the transistors used in LCDs with equivalent-sized pixels. However, as the current output from the transistor dictates the brightness of the pixel, the transistor to transistor uniformity must be very tight. Additionally, multiple OFETs are needed per OLED pixel, requiring OLED OFETs to be smaller than the OFETs used in EPDs, where only one OFET is required per pixel. This leads to the need for higher-mobility organic semiconductors as well as reduced transistor to transistor anisotropy to avoid issues of color shifts from differential pixel aging effects and nonuniform pixel brightness.

Higher-mobility semiconductor materials are also required, as future demand for larger screen sizes, better resolution, and faster refresh rates for video rate displays will lead to the need for higher ON currents as a result of the larger number of rows and columns, as well as the requirement for faster pixel charging speeds. The development of these materials is discussed in the next section.

1.2

Materials Properties of Organic Semiconductors

Organic semiconductors are based on the fact that the sp^2 hybridization of carbon in a double bond leaves a p_z orbital available for π bonding. The electrons in the π bond can be delocalized via conjugation with neighboring π bonds, thus giving rise to charge carrier mobility. For this reason, the majority of organic semiconductors are composed of aromatic units linked together, allowing π orbital conjugation along the length of the molecule. Charge transport within both small molecule and polymeric organic semiconductors generally occurs via a thermally activated hopping mechanism, and in an OFET, this occurs along the plane of the substrate, propagating within a thin layer of semiconductor only a few molecules thick at the dielectric interface. Thus, the semiconductor at this interface must be highly ordered into closely packed organized π stacks with correctly oriented and interconnected domains as illustrated in Figure 1.2. This can be achieved by utilizing coplanar aromatic molecules, which form a highly crystalline thin film microstructure domain leading to high charge carrier mobility.

Most high-performing semiconducting polymers exhibit a crystalline phase, melt transition, and amorphous phase on heating. The temperature at which the phase

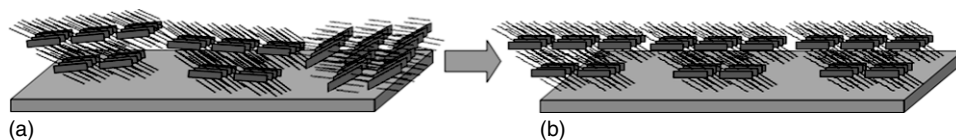


Figure 1.2 Schematic representation of (a) misaligned and poorly connected lamellar domains and (b) coaligned domains. Morphology in (b) leads to more optimal charge transport.

transition appears is dependent on the Gibbs free energy of each phase with respect to temperature, with the lowest free energy phase prevailing. Aromatic planar extended rigid-rod-type polymers have a predisposition to exhibit a liquid crystalline phase, due in part to their calamitic conformation. This phase is often masked by the lower free energy of the crystalline or amorphous phase. However, for some polymers, a liquid crystalline phase occurs between the crystalline and the isotropic melt phases (Figure 1.3). Annealing of the polymer within the liquid crystalline phase produces highly ordered and aligned crystalline thin films, which is desirable for high charge carrier mobilities. So in order to design polymers that incorporate a liquid crystalline phase, the entropy (dg/dT) of the isotropic phase must be decreased. This can be achieved by increasing the stiffness of the polymer backbone by the use of coplanar aromatic molecules, which decreases the disorder of the melt (decreased slope of dg/dT), allowing the liquid crystalline phase to appear.

The molecular weight of polymers also has an influence on the charge carrier mobility [7]. Increasing the molecular weight has been shown [8, 9] to be beneficial up to a plateau region, and so average molecular weights above 20 kDa are typically desired. The reason for this is that high polymer molecular weights enable the crystalline domains within the transistor thin film to be better defined and more interlinked. On the other hand, low-molecular-weight polymer films, although they

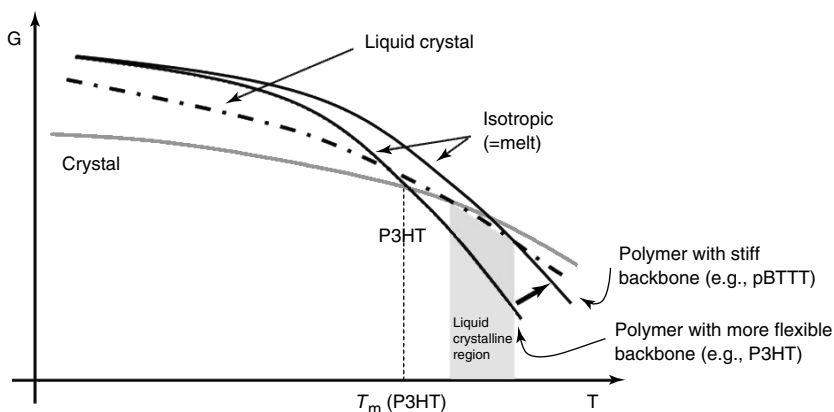


Figure 1.3 Effect of stiffening polymer backbone on the polymer-phase free energy.

exhibit higher crystallinity, they have more defined grain boundaries, thus leading to lower mobilities [10]. However, at very high molecular weights ($M_n > 150$ kDa), the polymer has a higher viscosity, which hinders the crystallization during annealing. This leads to reduced mobilities. Having a high polydispersity index, that is, a broad range of molecular weights is also expected to lead to reduced mobilities because of poor crystallization, although no systematic studies have investigated this so far [11].

Another consideration, in addition to the charge carrier mobility, is the stability of the semiconductor under ambient conditions. This has an impact on both the device lifetime as well as the device ON and OFF currents, as the introduction of bulk charge carriers through doping leads to an increase in the conductivity of the semiconductor when the gate voltage is off. The electrochemical stability of the organic semiconductor is dictated by the HOMO energy level of the molecule or polymer as redox electrochemistry with oxygen in the presence of water leads to the loss of electrons from the HOMO, provided that the HOMO is <4.9 eV from the vacuum energy level [12]. Thus, it is important to lower the HOMO energy level below this value through judicious molecular design of the molecule or polymer.

One distinction between small molecule semiconductors and polymeric semiconductors is in the way they can be processed. Small molecule semiconductors can be processed either by evaporation or using solution-based techniques. Polymeric aromatic semiconductors, however, cannot usually be processed by evaporation, so they must be functionalized to ensure that they are solution processable. As polymeric semiconductors designed for charge transport typically have closely packed stiff aromatic backbones, are highly crystalline, and have low polarity, they are usually insoluble in the majority of commonly used organic solvents. Thus, aliphatic side chains must be employed to enhance their solubility. The length, degree of branching, and density of the alkyl side chains influence both the vertically separated chains d spacing, and π stacking distances, which in turn affect the thin film morphology and consequently the transistor field-effect mobility. Both the formulation rheology and the thin film thermal properties can be controlled by tuning the polymer molecular weight and polydispersity, allowing compatibility with printing techniques such as flexography and gravure, which have high viscosity requirements. This allows control over the thickness and morphology of the conformal and cohesive thin films, minimizing thin film reticulation, which often occurs as the solution dries on a low-energy surface substrate. Solution deposition of multilayer device stacks is possible with polymeric semiconductors, as their limited solubility (narrow solubility parameter profile) and their high bulk viscosity enable solvent orthogonality. This is a prerequisite, as sequential solution deposition of one polymer layer on top of another requires that each deposited layer is inert to the solvents and temperature conditions that they are subsequently exposed to. Additionally, the negligible vapor pressure of polymers means that they are not susceptible to interlayer diffusion during the thermal cycles undertaken during device fabrication. The robust mechanical properties of polymeric thin films make them ideal for flexible processing or flexible substrate operation. As polymers crystallize forming crystalline domains, which are small relative to the transistor

channel length, fairly isotropic in-plane transport can be obtained. This leads to low device to device performance variability, which is important for applications where large numbers of transistors are integrated.

1.3

Small Molecule Semiconductors

1.3.1

Sexithiophene

Thiophene is an electron-rich planar aromatic heterocycle and its 2,5-coupled oligomers form well-ordered structures in thin films. One of the first promising thiophene-containing organic semiconductors was sexithiophene (6T) [13]. This oligomer showed mobilities in field-effect transistors of $10^{-3} \text{ cm}^2 \text{ V}^{-1} \text{ s}^{-1}$, which was the highest of any organic semiconductor at the time [14]. The rigid rod molecules of 6T were able to adopt an all-transplanar configuration because of the sulfur atoms arranging spatially along the length of the molecule to maximize their separation from each other across the short axis. As the angle formed between adjacent thiophene units linked at the positions 2 and 5 is $<180^\circ$, rotation of an individual thiophene unit around the long axis of the polymer is restricted due to the energetically unfavorable requirement that neighboring molecules will also need to rotate in a cooperative manner. Thus, the coupled thiophene units can adopt a coplanar conformation, allowing close intermolecular approach between neighboring backbones. For 6T, this results in a herringbone packing arrangement with relatively close $\pi-\pi$ distances, which in turn allows efficient intermolecular (or interchain) hopping of charges, leading to high charge mobility. However, one drawback of 6T is that it requires deposition from the vapor phase under vacuum in order for it to be processed [15] as it is scarcely soluble [16] and so is unsuitable for processing by high-throughput solution-based printing techniques.

1.3.2

Pentacene and Derivatives

Another small molecule that has been frequently employed in transistors is pentacene [17] with mobilities of up to $5 \text{ cm}^2 \text{ V}^{-1} \text{ s}^{-1}$ achieved for thin film devices whose processing conditions have been extensively optimised [18]. As pentacene is a planar acene molecule, it is also able to pack in a herringbone arrangement, thus giving rise to ordered, crystalline films, with high mobilities. However, it is poorly soluble in most solvents, except for hot chlorinated aromatics, and so also requires vapor deposition to form thin films. Thus to make pentacene more amenable to solution processing, Anthony and coworkers [19–22] have produced a number of pentacene derivatives. These involve the introduction of bulky alkynyl silyl groups at the positions central 6 and 13 of the pentacene ring, which have shown a marked improvement not only in solubility but also in oxidative stability. Additionally, the

crystal packing arrangement has been altered by the substituents, resulting in highly ordered two-dimensional slipped stack arrays being formed for certain derivatives of substituted pentacenes and related dithienoanthracenes. Recent work [23] has shown pronounced grain boundary effects on the charge transport of slip stacked crystal motifs in comparison to the more isotropic herringbone arrangements of pentacene. However, on optimizing processing conditions to form continuous polycrystalline thin films, these materials have given rise to impressive mobilities in excess of $1 \text{ cm}^2 \text{ V}^{-1} \text{ s}^{-1}$ [21, 24], which exceeds requirements for most initial organic electronics applications. Unfortunately, problems with these materials still persist, including the issues of anisotropic in-plane transport, which causes device to device nonuniformity, interlayer mixing upon solution deposition of multilayer stacks, and the difficulty in controlling the process of crystallization over large substrate areas. One method to overcome this is the use of small-molecule-polymer blends, which is discussed later in this chapter.

1.4

Polymer Semiconductors

1.4.1

Thiophene-Based Polymers

1.4.1.1 Poly(3-Alkylthiophenes)

Thiophene-containing polymers have emerged as leading examples of high-performing semiconductors. These polymers are typically electron rich, with lamellar microstructures exhibiting closely packed π -stacked backbones, optimal for charge transport. In this chapter, we review three examples of this class of polymer, shown in Figure 1.4.

Regioregular (RR) poly(3-hexylthiophene) (P3HT) is the most extensively studied semiconducting polymer. This is not only due to its ease of processing from solution and the fact that it is widely available but also due to its highly crystalline microstructure that gives rise to its promising electrical properties. It has been shown that a systematic improvement in charge carrier mobility can be obtained

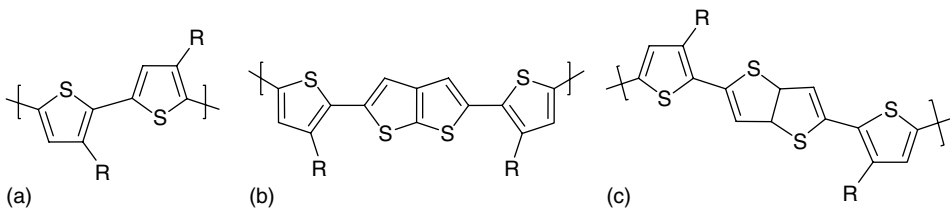


Figure 1.4 Structure of thiophene polymers (a) poly(3-hexylthiophene) (P3HT), (b) poly(2,5-bis(3-alkylthiophen-2-yl)thieno[2,3-*b*]thiophene) (pBTCT), and (c) poly(2,5-bis(3-alkylthiophen-2-yl)thieno[3,2-*b*]thiophene) (pBTTT).

by maximizing the regioregularity and the molecular weight of the polymer. The effect of increased regioregularity is to avoid out-of-plane twists along the backbone of the polymer, as monomers in a head to head orientation experience steric repulsions between adjacent alkyl groups. This disrupts the planarity of the molecule, decreasing the effective conjugation length of the polymer, as can be seen in the hypsochromatic shifts in optical absorbance as the regioregularity decreases [25]. This in turn reduces the efficiency of charge hopping. P3HT with a head to tail regioregularity in excess of 96% has been shown to exhibit charge carrier mobilities of up to $0.1 \text{ cm}^2 \text{ V}^{-1} \text{ s}^{-1}$ under inert atmospheric conditions [26]. Indeed, there are still efforts to further push the measured transistor mobilities through improvements in processing conditions, device architecture, and electrodes [27–30]. On changing the molecular weight of the polymer, atomic force microscopy (AFM) measurements show that low-molecular-weight high-RR P3HT ($\sim 5 \text{ kDa}$) forms highly crystalline rodlike structures in which the width of the rod does not exceed the length of the individual polymer chains. RR P3HT with higher molecular weights ($> 30 \text{ kDa}$) exhibits less crystallinity with small nodule like crystallites interconnected with amorphous regions. The higher-molecular-weight RR P3HT shows higher mobilities than the more crystalline low-molecular-weight RR P3HT films. One explanation for this is that the higher-molecular-weight P3HT has better defined and more connected grains allowing better intergrain charge transport, whereas the low-molecular-weight RR P3HT has more defined grain boundaries [10]. Another explanation for the reduced mobility in low-molecular-weight films cites enhanced out-of-plane twisting in the polymer chains, leading to shorter conjugation lengths and thus reduced charge hopping rates [31]. Studies have also correlated increasing molecular weight with increasing crystalline quality within domains, in the high-mobility regime, as there are fewer chain ends per domain, as well as the possibility for individual polymer chains to interconnect domains at high molecular weight [9]. However, there is a limit to the improvements on increasing the molecular weight, as at over $\sim 50 \text{ kDa}$, crystalline disorder increases, a phenomenon that can be attributed to slower crystallization kinetics.

Studies regarding the alkyl side chain influence on the electrical performance of polyalkylthiophenes have been undertaken by several groups. These studies indicate that hexyl side chains are the optimum length, as the charge carrier mobility decreases as the chain length increases [32–34]. As the face to face ($\pi-\pi$) distance is similar across the series of polymers fabricated [35], it is apparent that the decrease in charge carrier mobility may be due to the increase in the fraction of insulating side chains in the polymer. If the polymer lamellae are misaligned in the plane of the substrate and the direction of charge flow, then hopping or tunneling between the insulating alkyl side chains will be necessary for charge transport. However, as hopping rates are dependent on the distance between neighboring polymer chains, longer alkyl side chains would be expected to be detrimental to charge mobility.

The effect of bulky or highly polar substituted end groups on the side chains has been studied by Bao and Lovinger [35]. The series of RR polythiophenes prepared

showed poor field-effect mobilities of around $10^{-6} \text{ cm}^2 \text{ V}^{-1} \text{ s}^{-1}$ because of the low degrees of crystallinity and ordering exhibited. The incorporation of chiral alkyl side chains was shown to maintain crystallinity at the expense of the π - π stacking distance – the distance was increased to 4.3 Å as opposed to 3.8 Å for P3HT. This led to a decrease in charge carrier mobility of around one order of magnitude. The overall findings of the study showed that nonpolar linear alkyl chains were optimal for charge transport because of the efficient backbone stacking.

The HOMO energy level of P3HT is about -4.6 eV from the vacuum energy level as a consequence of the electron-rich, π -conjugated, highly planar aromatic backbone that has electron-donating alkyl side chains. This HOMO level renders P3HT potentially unstable to ambient air and humidity, as electrochemical oxidation occurs at potentials above -4.9 eV [12]. Even though the sensitivity to water and oxygen redox electrochemistry is not the only contributing factor to the instability of P3HT, as well as for other π -conjugated aromatics, it is crucial to ensure that the electrochemical oxidation of the organic semiconductor is not thermodynamically favorable. There are a number of reports in the literature that have observed instabilities in OFET performance under ambient air conditions [36, 37] and have credited this to an interaction with molecular oxygen [38]. For instance, charge-transfer complexes between oxygen and thiophene have been proposed, which can generate reversible charged states and show a doping effect on transistor performance.

On photoexcitation, singlet oxygen can be generated by energy transfer from excited electronic states, which causes irreversible chemical degradation to the polymer. The mechanism of this photooxidation is that the singlet oxygen undergoes a 1,4-Diels-Alder addition reaction to the thienyl double bonds of the thiophene ring, breaking the conjugation of the backbone. However, in the absence of light, oxygen is not a strong oxidant for thiophene polymers. Instead, ozone, and possibly other pollutants such as NO_x and SO_x found in ambient air, have high electron affinities and are likely to participate in doping [39]. If the ozone molecule stays intact during the complexation with the polymer, then the doping is reversible. Irreversible doping occurs when, on dissociation, an exothermic reaction between the polymer and the ozone molecule occurs, cleaving the carbon-carbon bonds in the backbone, leading to reduced conjugation. This rationalization for organic semiconductor instability is consistent with the evidence that top-gate devices usually display enhanced stability in comparison with bottom-gate devices [40]. In a top-gate device architecture, the organic semiconducting layer is protected from the environment by the dielectric and gate layers, which potentially act as sacrificial layers for reactions with highly reactive dopants such as ozone.

There are many synthetic design parameters that affect the performance of the semiconductor. Polydispersity [41], molecular weight [10, 31, 42–46], levels of impurities [47], end groups, and chemical defects in the polymer backbone [48–50] are all important, as they influence both the morphology and electrical properties of the organic semiconductor within the devices. All these parameters are affected by the choice of the polymerization conditions, with the final purification steps being able to control the polydispersity, molecular weight, and impurities

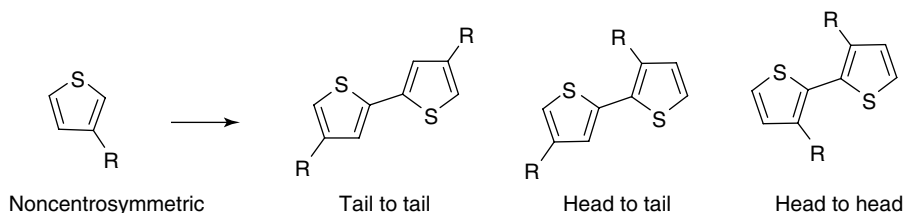


Figure 1.5 Possible regiochemistries from the dimerization of a noncentrosymmetric thiophene monomer.

to some extent. However, it is usually not possible to remove chemical defects in the polymer backbone, and so these are best avoided by carefully choosing and optimizing an appropriate synthetic route. As the monomers used for the synthesis of poly(3-alkylthiophenes) are noncentrosymmetric, the regiochemistry of the solubilizing side chains is difficult to control. One of the most studied examples is the polymerization of halogenated 3-hexylthiophene monomer to produce P3HT. Here, there are three possible products that can be formed, tail to tail, or head to tail, or head to head, as shown in Figure 1.5. For poly(3-alkylthiophenes), great progress in optimizing the regioregularity and polymer molecular weight has been made over the years by employing a number of different synthetic routes [51–57].

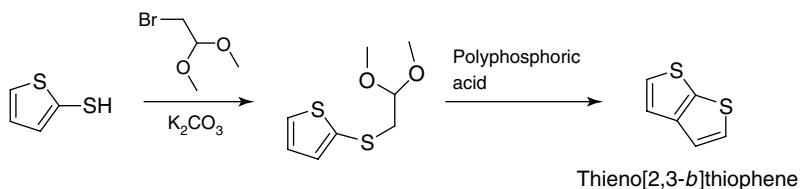
1.4.1.2 Thienothiophene Copolymers

The majority of design strategies to reduce the susceptibility of thiophene polymers to degradation or oxidative doping involves decreasing the HOMO energy level below the electrochemical oxidation threshold [58]. As the number of conjugated units along the backbone increases, the HOMO energy level increases up to a critical conjugation length, at which point it remains fairly constant. However, the conjugation length of the backbone can be controlled either by changing the coplanarity (more coplanar π orbitals promote increased delocalization) and therefore the π orbital overlap between neighboring thiophene rings or electronically by introducing a repeat unit into the backbone, which inhibits or prevents π orbital delocalization. The HOMO energy level also increases when the electron density of the conjugated π system is increased.

In the alternating copolymer thieno[2,3-*b*]thiophene and 4,4'-dialkyl-2,2'-bithiophene referred to as poly(bithiophene-cross-conjugated thiophene (pBTCT), the thieno[2,3-*b*]thiophene is a π orbital conjugation blocker, as the central cross-conjugated double bond prevents conjugation between the substituents at the positions 2 and 5. Thus, full conjugation along the backbone is not permitted [59], leading to a lower lying HOMO (larger ionization potential). Additionally, the reduced number of electron-donating chains per aromatic group also contributes to the lower lying HOMO. Ultraviolet photoelectron spectroscopy (UPS) has confirmed that the pBTCT polymer series, composed of pBTCT with alkyl chain lengths from C8 to C12, exhibit a 0.4 eV lowering of the HOMO energy level in comparison to P3HT [60]. The strategy employed for pBTCT synthesis

used a regiosymmetrical backbone repeat unit, which was polymerized by Stille coupling. This prevents regioisomerism, which can produce conformational irregularities and in turn reduce crystallinity. The backbone conformation that is most energetically favorable for pBTCT is a “crankshaft” conformation in which the sulfurs in neighboring monomer units arrange in an “anti” configuration because of their large size, which requires them to maximize their spatial separation. The alkyl side chains have two different separation distances on the backbone, which are wide enough to enable side chain interdigitation between the neighboring polymer chains, unlike in P3HT where the side chain packing density is too high to allow interdigitation. As the thieno[2,3-*b*]thiophene monomer unit is planar, pBTCT is able to adopt a coplanar conformation, with the alkyl side chains arranged in a tail-to-tail regiosymmetrical arrangement along the backbone. This repositioning of the alkyl groups ensures that there are no steric interactions between adjacent alkyl chains, enabling pBTCT to have a highly planar backbone conformation with optimal π orbital overlap and delocalization within the bithiophene. The backbone planarity is evident from high-resolution grazing X-ray scattering measurements that show interchain π – π stacking distance of 3.67 Å, which is 0.13 Å less than that of P3HT, as well as charge carrier mobilities of $0.04 \text{ cm}^2 \text{ V}^{-1} \text{ s}^{-1}$. ON/OFF ratios of around 10^6 have been obtained in air, with devices showing only very minor changes in transfer characteristics when measured over a two-month period [60]. This oxidative stability can be attributed to the lowering of the HOMO energy level as previously mentioned.

The thieno[2,3-*b*]thiophene monomer unit has been synthesized in a variety of ways [61–63]. One example is the elegant synthesis reported by Otsubo *et al.*, in which 1-trimethylsilylpentadiyne is lithiated with *n*-BuLi/BuOK, followed by trapping of the created anion with carbon disulfide [62], producing 2-trimethylsilylthieno[2,3-*b*]thiophene, as a result of the ring closure reaction that occurs during the workup, and is further desilylated upon treatment with tetrabutylammonium fluoride to give thieno[2,3-*b*]thiophene [63]. A more convenient route (Scheme 1.1) has been developed for larger-scale reactions in which commercially available 2-thiophenethiol is used as the starting material (Scheme 1.1) [64]. Alkylation using bromoacetaldehyde dimethyl acetal under Williamson ether conditions yields the protected aldehyde, which on deprotection can be ring closed under



Scheme 1.1 Synthesis of thieno[2,3-*b*]thiophene.

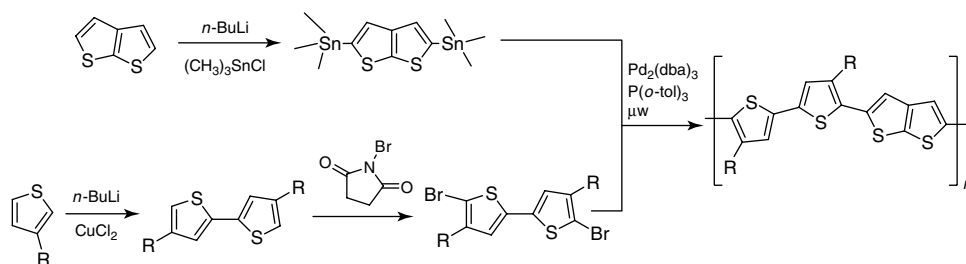
reflux with phosphoric acid in chlorobenzene. This affords thieno[2,3-*b*]thiophene as a colorless oil.

There are generally two approaches to the synthesis of regiosymmetric polymers, the homopolymerization of a suitable centrosymmetric monomer and polymerization of two difunctional symmetric monomers (a so-called AA + BB approach), to produce an alternating copolymer. The benefit of the AA + BB approach is that a variety of copolymers can be synthesized purely by changing one of the comonomers in the polymerization. However, the disadvantage of this approach is that the molecular weight of the polymer is governed by the Carothers equation, so in order to achieve high molecular weights, a strict 1 : 1 stoichiometry needs to be maintained to achieve a high degree of reaction conversion. In practice, this means that only high yielding cross-coupling chemistries are suitable for this approach, and very-high-purity crystalline monomers are necessary to obtain high molecular weights [65].

pBTCT can be synthesized according to the AA + BB methodology using Stille cross-coupling (Scheme 1.2). 2,5-Trimethyl(stannyl)thieno[2,3-*b*]thiophene is readily prepared by lithiation of thieno[2,3-*b*]thiophene with 2 equiv. of *n*-butyllithium, followed by quenching of the resulting dianion with trimethylstannyl chloride. The choice of using trimethyltin as the organometallic group, in spite of its high toxicity, is because it affords a highly crystalline product that can be readily purified. The trimethylstannyl monomer has been polymerized with a range of 5,5-dibromo-4,4-dialkyl-2,2-bithiophenes in the presence of a palladium catalyst to afford polymers with typical weight average molecular weights of around 50–60 000 g mol⁻¹ and polydispersities of around two [11].

1.4.1.3 pBTCT

An analogous copolymer to pBTCT is poly(2,5-bis(3-alkylthiophen-2-yl)thieno[3,2-*b*]thiophene (pBTCTT) composed of alternating thieno[3,2-*b*]thiophene and 4,4-dialkyl 2,2-bithiophene monomer units [66, 67]. The difference between the two copolymers is that the thieno[3,2-*b*]thiophene monomer has a different arrangement of double bonds in comparison to thieno[2,3-*b*]thiophene, as the sulfur atoms are arranged in an “anti” orientation as opposed to “syn.” This allows conjugation between the neighboring thiophenes at the positions 2 and 5, thus enabling extended π



Scheme 1.2 Polymerization of pBTCT.

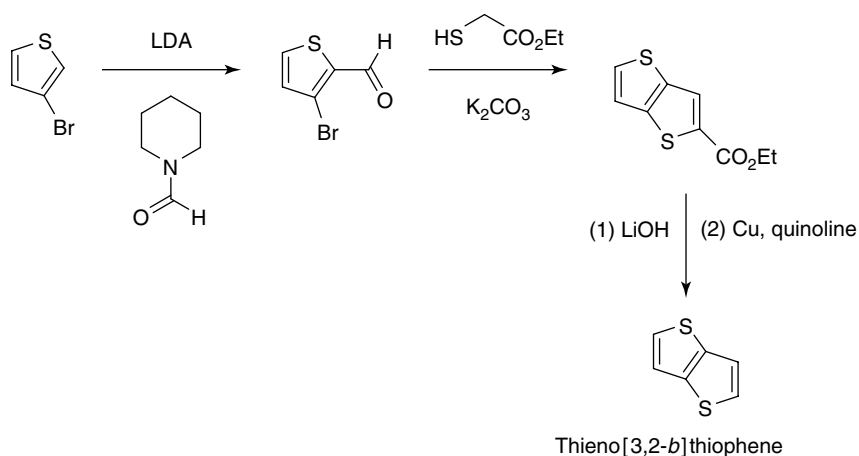
orbital delocalization along the polymer backbone. In turn, this leads to a lower bandgap and ionization potential than pBTCT. As is the case with pBTCT, pBTIT has alkyl groups solely on the bithiophene units. These alkyl groups inductively donate σ electron density into the π electron system of the polymer backbone, raising the HOMO energy level. However, the fact that there are fewer alkyl groups per unit length in the polymer backbone compared to P3HT, because of the unsubstituted thieno[3,2-*b*]thiophene units, means that the HOMO energy level is lower than P3HT. In addition, the aromatic thieno[3,2-*b*]thiophene ring has a larger resonance stabilization energy than a thiophene ring, as the quinoidal form of the fused ring has a higher energy and is thus less favorable. The consequence of this is to decrease the delocalization of electron density from the aromatic thieno[3,2-*b*]thiophene ring, reducing delocalization along the polymer backbone and thus lowering the HOMO energy level, giving rise to improved ambient operational stability. The backbone of pBTIT adopts a planar conformation as the planar monomers, both of which are centrosymmetric, have an all “anti” sulfur arrangement across the short axis. This enables main chain extension as a “rigid rod” shape, with the monomer units alternately bending to accommodate the nonlinear bond angle between neighboring thiophene units. As the side chain attachment density along the polymer chain is low and the symmetry of the repeat units allows them to rotate around the backbone axis, the alkyl side chains are able to interdigitate with the alkyl groups of neighboring polymer chains. Additionally, the long-range linearity of the polymer backbone facilitates backbone π stacking, enabling neighboring polymer backbones to assemble in a closely packed, tilted face-to-face arrangement [68]. This creates an extended order microstructure, denoted as π -stacked lamella, in which the interdigitated side chains facilitate “registration” between the vertically π -stacked adjacent lamella, thus promoting the formation of large three-dimensional ordered domains.

pBTIT polymers exhibit a thermotropic liquid crystalline phase, which originates on heating when the side chains melt. Transitions in differential scanning calorimetry (DSC) experiments show that the mesophase persists until a further main chain melting thermal transition occurs. As fairly high melting enthalpies are observed, it is evident that the polymers exhibit a high level of crystallinity of both side and main chains, as is consistent with the model of an interdigitated, closely packed polymer conformation. Thermal annealing within the mesophase can further develop the lamella microstructure to create well-connected three-dimensional polycrystalline thin films. Combining thermal annealing with low-energy surface treatments such as with hexamethyldisilazane (HMDS), which forms a self-assembled monolayer (SAM) on the substrate surface, promotes the edge on orientation of the polymer backbone along the surface [69, 70]. This allows the growth of highly ordered crystalline domains, and the coalignment of the domains by the low-energy surface promotes good intergrain connectivity. The effect of annealing on the ordering and orientation of the polymer has been shown by two-dimensional grazing incident X-ray diffraction studies [71] to improve both the crystallinity of the film by forming larger grain sizes, enhance in-plane orientation, and reduce the lamellar spacing from 19.5 to 19.2 Å. This has the effect

of increasing the charge carrier mobility and has led to devices with high hole mobilities of up to $1 \text{ cm}^2 \text{ V}^{-1} \text{ s}^{-1}$ in OFET devices under N_2 [72].

The thieno[3,2-*b*]thiophene monomer can be synthesized from commercially available 3-bromothiophene in four steps. Lithiation of the 3-bromothiophene at the position 2 with diisopropylamine (LDA), a nonnucleophilic base, followed by quenching of the resulting anion with *N*-formylpiperidine or dimethylformamide produces *o*-bromoaldehyde. Reacting this thiophene aldehyde with ethyl 2-sulfanylacetate in conjunction with a base produces a good yield of substituted thieno[3,2-*b*]thiophene. The ester group is converted to a carboxylic acid by hydrolysis, which is subsequently removed by thermal decarboxylation with quinoline in the presence of copper. This produces the unsubstituted thieno[3,2-*b*]thiophene with an overall yield of 60% over the course of the four steps (Scheme 1.3) [73, 74].

Like pBTCT, pBTTT can be synthesized using the AA + BB strategy. Lithiation of thieno[3,2-*b*]thiophene at the positions 2 and 5 with 2 equiv. of *n*-butyllithium, followed by quenching with trimethyltin chloride affords the difunctional tin monomer. Stille coupling of the trimethylstannyl monomer with a range of 5,5-dibromo-4,4-dialkyl-2,2-bithiophenes using a palladium catalyst produced a crude pBTTT polymer, which was purified. Purification involved the precipitation of the polymer from the reaction solvent, followed by solvent extraction to remove low-molecular-weight oligomers and the catalyst. For pBTTT, it was possible to remove traces of metal catalyst via chromatographic purification by filtration over a plug of silica, a process that is unusual for the purification of most polymers. Reprecipitation into acetone, a nonsolvent in this case typically gave the polymer in 90% yields, with molecular weights in the range of 20–30 000 g mol^{-1} , depending on the length of the alkyl side chains, with polydispersities of around two.



Scheme 1.3 Synthesis of thieno[3,2-*b*]thiophene.

1.5 Semiconductor Blends

Two or more organic semiconductors within a blend film can be used to combine the advantageous properties of each component. As previously mentioned, the processability of small molecular semiconductors is generally lower than that of polymers; however, control of crystallization and increased film uniformity can be achieved using a polymer-small-molecule blend while retaining high charge carrier mobilities. Other benefits to using blends include the ability to combine n- and p-type materials within the same film and the possibility for self-assembly from solution of the device constituents. Although the range of possible film microstructures increases with the addition of more components, this added complexity is often outweighed by the ease with which certain features such as film uniformity, processability, ambipolarity, solubility, and environmental stability can be combined.

There have been several examples of blend OFETs designed for high mobility and ease of processing. First, the use of crystalline-crystalline polymer systems, where RR P3HT and common bulk polymers such as poly(styrene) are blended, allows low concentrations of the semiconducting component and improved mechanical properties [75]. Second, polymer-small-molecule systems, based on both oligothiophenes and acenes, have been solution processed for OFETs. In the case of 2,8-difluoro-5,11-bis(triethylsilylethynyl) anthradithiophene blended with poly(triarylamine), mobilities of well over $2 \text{ cm}^2 \text{ V}^{-1} \text{ s}^{-1}$ have been demonstrated [76]. The key to understanding these systems and the behavior of many blends is the phase separation of the components. Owing to the low entropy of mixing of polymer-polymer systems and even small-molecule-polymer systems, phase separation in many organic systems is thermodynamically favorable. However, during solution processing, such as spin coating, the system is often far from equilibrium and the solvent itself will strongly affect the final film morphology. Thus, solvent evaporation rates, substrate-solution interactions, solution viscosities, and solute-solvent interactions (or solubility) are all important factors. Phase separation can occur both laterally and/or vertically within a thin film because of the presence of interfaces. Thus, it is possible to control the location of a component within the blend film and, in particular, increase the concentration of high-mobility material at the semiconductor-dielectric interface. This has been achieved by vertical phase separation in, for example, acene-polymer blend OFETs in a top-gate architecture. Similarly, in crystalline polymer blends, the process of crystallization-induced phase separation can lead to semiconductor accretion at the interfaces and therefore allows electrical percolation even at very low semiconductor concentrations. In this case, the order of solidification of the components during processing is critical to obtaining the correct morphology. Controlling crystallization by annealing after film deposition is also possible using a glass-forming additive. This has been demonstrated in a rubrene blend [77] and allows for improved processability in the amorphous state and high mobilities after annealing.

1.6 Device Physics and Architecture

The design of an OFET can be one of the four different architectures depending on whether the gate electrode is deposited prior or after the semiconductor layer and whether the source and drain electrodes are in the same plane as the dielectric (coplanar) or not (staggered) (Figure 1.6). These can affect the ease of device manufacture and the final performance of the device. A bottom-gate, bottom-contact geometry is commonly employed because it allows simple screening of new materials, is well established for display backplane applications, and is easy to fabricate. However, coplanar architectures do not usually give the optimal performance since improved gate-field-enhanced charge injection is present in staggered electrode devices. For all geometries, a simple thin film model that was first developed for inorganic transistors can be applied [78]. Despite the differences between inorganic and organic electronics, the model has been widely employed and allows the estimation of field-effect mobilities. Deviations from this ideal model arise in OFETs because of contact resistances [79] and electric-field-dependent mobilities [80].

If we consider a three terminal device with source, drain, and gate, the gate is separated from the semiconductor by a dielectric layer, and charge carriers are injected into the semiconductor from the source. The source is normally grounded

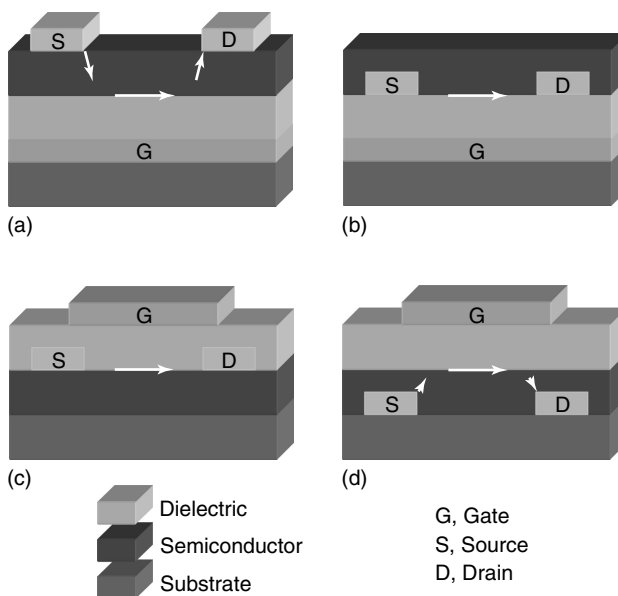


Figure 1.6 OFET device architectures: (a) top contact, bottom gate; (b) bottom contact, bottom gate; (c) top contact, top gate; and (d) bottom contact, top gate. Arrows represent the charge carrier pathways in the device and show the difference between staggered and coplanar arrangements.

and the drain voltage, V_D , is used to induce a source-drain current, I_D , which in turn is modulated by the gate field caused by V_G . It is well established that OFET conduction occurs within a few monolayers of material, essentially in a two-dimensional fashion at the semiconductor–dielectric interface [81]. If we first consider the resistance, dR , of a thin element of the channel, dx , we obtain,

$$dR = \frac{dx}{WQ(x)\mu} \quad (1.1)$$

where W is the channel width, μ is the charge carrier mobility, and $Q(x)$ is the surface charge density at point x (Figure 1.7).

The magnitude of this charge depends mainly on the applied gate voltage and the voltage at x due to V_D ; however, in addition, there will be a threshold voltage, V_T , that accounts for the flat-band potential, for the charge donor or acceptor state present, and/or for charge trapping of injected carriers. Hence, we can express $Q(x)$ in terms of these voltages and the geometric capacitance of the dielectric layer, C_i ,

$$Q(x) = C_i[V_G - V_T - V(x)] \quad (1.2)$$

Several assumptions are needed in order to calculate the current through the channel. Firstly, we take the mobility to be independent of voltage and thus x , and secondly, we use the gradual channel approximation, that is, the channel length is much greater than the film thickness so that the perpendicular electric field is greater than that in the x -direction. Substituting into $dV = I_D dR$ and integrating over the channel length, L , gives

$$I_D = \frac{W}{L} \mu C_i \left[(V_G - V_T) V_D - \frac{V_D^2}{2} \right] \quad (1.3)$$

This is the general form of the equation for I_D , but we can apply it to the two regimes of the OFET, namely, linear and saturation. In the linear regime $V_G - V_T \gg V_D$, the accumulation region is uniform along the channel, and hence,

$$I_{D \text{ lin}} = \frac{W}{L} \mu C_i (V_G - V_T) V_D \quad (1.4)$$

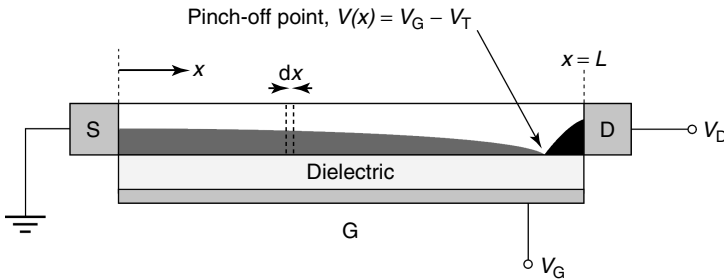


Figure 1.7 Schematic diagram of an OFET channel of length, L , showing source (S), drain (D), and gate (G) electrodes. The accumulation layer is represented in dark grey, and saturation occurs when pinch-off of this region leads to a region next to the drain that is depleted of carriers. At this point, $V_{D \text{ sat}} = V_G - V_T$.

In the saturation regime where pinch-off of the accumulation region occurs and $V_{D \text{ sat}} = V_G - V_T$, we have

$$I_{D \text{ sat}} = \frac{W}{2L} \mu C_i (V_G - V_T)^2 \quad (1.5)$$

From these equations, we can therefore calculate the field-effect mobility within the OFET as follows

$$\mu_{\text{lin}} = \frac{L}{WC_i V_D} \left(\frac{\partial I_{D \text{ lin}}}{\partial V_G} \right) \quad (1.6)$$

$$\mu_{\text{sat}} = \frac{L}{WC_i} \left(\frac{\partial I_{D \text{ sat}}}{\partial V_G} \right) = \frac{2L}{WC_i} \left(\frac{\partial \sqrt{I_{D \text{ sat}}}}{\partial V_G} \right)^2 \quad (1.7)$$

Although these expressions are widely used, they contain an error if the intrinsic mobility is a function of the gate voltage [82] (or equivalently the charge density), which is common for organic semiconductors. Therefore, several other estimates for mobility can be used that, for example, do not incorporate the fitting parameter V_T but use the more physically meaningful onset voltage, V_{on} . One example would be the effective or average mobility, μ_{EFF} , calculated from Eq. (1.4) but considering all charges rather than just those when $V_G > V_T$.

$$\mu_{\text{EFF}}(V_G) = \frac{L}{WC_i V_D} \frac{I_{D \text{ lin}}}{(V_G - V_{\text{on}})} \quad (1.8)$$

When optimizing the electrical performance of OFETs, there are several factors to be considered. High charge carrier mobility is often important since higher currents are possible for fixed transistor dimensions. Also, the switching speed of integrated circuits increases with increased mobility [83]. These are key features for the driving circuitry in organic active matrix displays where high currents are needed to operate the OLEDs and small transistors are preferable compared to the pixel size in the case of bottom-emission devices. An often-quoted aim for OFETs is to achieve mobilities equal to or greater than that of a-Si, which is widely used for display backplanes. Owing to the weaker interactions between organic molecules than the covalent inorganic semiconductors, charge transport is rarely bandlike in nature. Instead, charges, which may well be polaronic [84], that is, distort their own molecular environment, are limited by hopping from one spatial region to another or by escaping from trap states. This leads, in most cases, to a thermally activated μ with only a few exceptions [85, 86]. Combined with the problems of charge injection from metallic electrodes and the nature of the semiconductor–dielectric interface, this makes the design of high-mobility OFETs challenging. The other main parameters that have an influence on the use of OFETs in circuits are the threshold voltage, V_T , and the *ON/OFF ratio* (defined as the ratio of currents between the on and off states of the device). Threshold voltages close to zero indicate negligible charge trapping or doping and are generally advantageous since large gate voltages are not required to switch the device on or off. A high ON/OFF ratio is also useful, as the leakage through the transistor, when it is in the off state, is minimized. If being used to charge a capacitor in, for example, a display application, this is particularly important.

The ON/OFF ratio can be approximated when there is negligible charge depletion by

$$\frac{I_{\text{ON}}}{I_{\text{OFF}}} = 1 + \frac{\mu C_i V_D}{2\sigma_{\text{bulk}} t} \quad (1.9)$$

where σ_{bulk} is the conductivity of the bulk film and t is the film thickness [87]. Thus, by reducing conduction through the bulk of the device, the off current can be lowered. In this respect, high mobilities, thin films, and low defect/impurity concentrations are essential for high ON/OFF ratios. Typical device characteristics for a high-mobility OFET are shown in Figure 1.8, demonstrating both linear and saturation regimes of the device as well as highlighting ON and OFF currents, threshold voltage, and onset voltage.

The performance of an OFET depends not only on the semiconducting material employed but also critically on the interfaces that this material makes with both the source and drain electrodes and the dielectric material. First, we must be able to inject and extract electrons or holes to and from the metallic contacts. When a metal and an organic semiconductor are placed in contact, there is an equalization of fermi levels in a similar fashion to inorganic materials. Electrons (holes) must then overcome any energetic barrier created for injection from the metal into the LUMO (HOMO) of the organic material. However, unlike inorganics, the magnitude of this barrier depends not only on the work function of the metal, ϕ_m , but also on the strength of the interaction between organic and metal and the possible creation of interface dipoles [88], leading to a shift in vacuum levels, Δ . Thus, instead of the

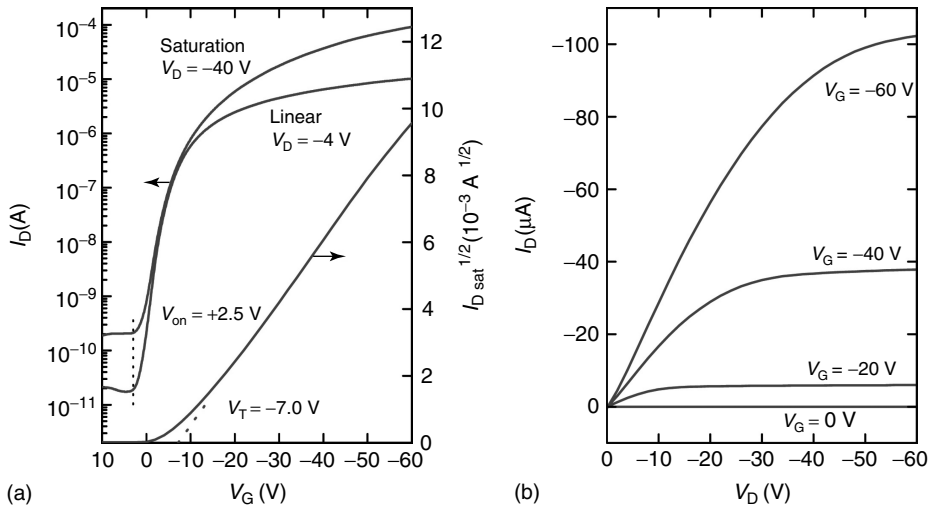


Figure 1.8 (a) Transfer and (b) output characteristics from a typical high-mobility p-type blend OFET. The channel length and width are 70 and 1000 μm , respectively, and mobility in the saturation regime can be calculated to be $2.5 \text{ cm}^2 \text{ V}^{-1} \text{ s}^{-1}$.

Mott–Schottky limit for electron injection, which gives a barrier height, ϕ_B , of

$$\phi_B = \varphi_m - \chi \quad (1.10)$$

with χ being the electron affinity of the semiconductor, that is, the position of the LUMO, we obtain

$$\phi_B = \varphi_m + \Delta - \chi \quad (1.11)$$

By selecting a suitable metal with a work function close to either the HOMO or LUMO energies of the organic material and/or by controlling interface dipole formation, the device performance can be made nonlimited by charge injection rates. An often-used technique to modify this interface is the application of SAMs to the metal. This involves the use of small organic molecules, such as thiols for metals [89], that can chemically bind to surfaces in such a way that a single, uniform layer forms. If the molecule has a dipole moment, it can alter Δ depending on its orientation to the surface or it can modify the surface energy and thus the interaction of the subsequent organic layer with the substrate.

The second important interface in an OFET is between the dielectric and semiconductor, where the accumulation layer forms and the majority of charge conduction occurs. Again SAMs are often employed to optimize this interface, especially with regard to minimizing charge trapping and modifying film morphology. The choice of dielectric itself, its surface properties, and its dielectric constant will play a key role in device operation. Some examples include the use of low permittivity polymeric materials to reduce energetic disorder at the interface [90] and the use of silane SAMs to passivate oxide dielectrics [91]. Layers with a large value of C_i are also potentially important for reducing the operating voltage of the OFET, key to realizing portable, low-power organic electronics. In this case, the SAM itself can be used as the dielectric such as long chain alkyl phosphonic acids on thin aluminum oxide [92].

1.7

Summary

One of the main advantages of organic electronics is the ability to produce large-scale circuits relatively cheaply and on a wide variety of surfaces such as flexible substrates. Fabrication using solution-based deposition including printing is one way to achieve this. However, there are several constraints when using organic materials in this way. Firstly, the majority of the processing must occur at low temperatures (typically $\lesssim 200^\circ\text{C}$) to prevent chemical decomposition. Secondly, designing materials that are easily processable can compromise their electrical performance. Thirdly, patterning of organics requires new techniques such as nanoimprinting, self-aligned printing, self-assembly, or soft lithography to make suitable device structures while keeping fabrication costs low. Finally, deposition of several materials is needed for even the most simple of devices, and thus one layer must not, for example, dissolve previous layers. The process of material deposition

will often strongly affect the microstructure of the solid film produced and therefore also the electrical properties of the OFET. Most solution deposition methods will be far from equilibrium, and the rates of solvent evaporation, material surface energies, and solution viscosities will influence film morphology. Over the past several years, many materials systems have been developed that aim to improve ease of processing while forming highly controllable or ordered thin films on a microstructural and/or molecular level. When employing these materials in organic devices, other factors such as interface effects, environmental stability, and device uniformity must then be considered and incorporated. Therefore, a combination of good electrical performance, device architecture, and material properties is needed in order to fabricate high-performance organic electronic devices suitable for possible commercial applications.

References

1. Horowitz, P. and Hill, W. (1990) *The Art of Electronics*, 2nd edn, Cambridge University Press.
2. Gelinck, G.H., Huitema, H.E.A., Van Veenendaal, E., Cantatore, E., Schrijnemakers, L., Van der Putten, J., Geuns, T.C.T., Beenhakkers, M., Giesbers, J.B., Huisman, B.H., Meijer, E.J., Benito, E.M., Touwslager, F.J., Marsman, A.W., Van Rens, B.J.E., and De Leeuw, D.M. (2004) *Nat. Mater.*, **3**, 106–110.
3. Loo, Y.-L. (2007) *AIChE J.*, **53**, 1066–1074.
4. Sirringhaus, H. (2005) *Adv. Mater.*, **17**, 2411–2425.
5. Gundlach, D.J., Royer, J.E., Park, S.K., Subramanian, S., Jurchescu, O.D., Hamadani, B.H., Moad, A.J., Kline, R.J., Teague, L.C., Kirillov, O., Richter, C.A., Kushmerick, J.G., Richter, L.J., Parkin, S.R., Jackson, T.N., and Anthony, J.E. (2008) *Nat. Mater.*, **7**, 216–221.
6. Gelinck, G.H., Huitema, H.E.A., van Veenendaal, E., Cantatore, E., Schrijnemakers, L., van der Putten, J.B.P.H., Geuns, T.C.T., Beenhakkers, M., Giesbers, J.B., Huisman, B.-H., Meijer, E.J., Benito, E.M., Touwslager, F.J., Marsman, A.W., van Rens, B.J.E., and de Leeuw, D.M. (2004) *Nat. Mater.*, **3**, 106–110.
7. Fumagalli, L., Binda, M., Natali, D., Sampietro, M., Salmoiraghi, E., and Di Gianvincenzo, P. (2008) *J. Appl. Phys.*, **104**, 084513/1–084513/8.
8. Chang, J.F., Sirringhaus, H., Giles, M., Heeney, M., and McCulloch, I. (2007) *Phys. Rev. B*, **76**, 205204–205215.
9. Chang, J.-F., Clark, J., Zhao, N., Sirringhaus, H., Breiby, D.W., Andreasen, J.W., Nielsen, M.M., Giles, M., Heeney, M., and McCulloch, I. (2006) *Phys. Rev. B: Condens. Matter Mater. Phys.*, **74**, 115318/1–115318/12.
10. Kline, R.J., McGehee, M.D., Kadnikova, E.N., Liu, J., Frechet, J.M.J., and Toney, M.F. (2005) *Macromolecules*, **38**, 3312–3319.
11. Iain, M., Martin, H., Michael, L.C., Dean, D., Kline, R.J., Michael, C., Warren, D., Daniel, F., David, G., Behrang, H., Rick, H., Lee, R., Alberto, S., Maxim, S., David, S., Steven, T., and Weimin, Z. (2009) *Adv. Mater.*, **21**, 1091–1109.
12. de Leeuw, D.M., Simenon, M.M.J., Brown, A.R., and Einerhand, R.E.F. (1997) *Synth. Met.*, **87**, 53–59.
13. Horowitz, G., Fichou, D., Peng, X., Xu, Z., and Garnier, F. (1989) *Solid State Commun.*, **72**, 381–384.
14. Horowitz, G., Fichou, D., Peng, X.Z., Xu, Z.G., and Garnier, F. (1989) *Solid State Commun.*, **72**, 381.
15. Wittmann, J.C., Straupé, C., Meyer, S., Lotz, B., Lang, P., Horowitz, G., and Garnier, F. (1997) *Thin Solid Films*, **311**, 317–322.

16. Sotgiu, G., Zambianchi, M., Barbarella, G., and Botta, C. (2002) *Tetrahedron*, **58**, 2245–2251.
17. Horowitz, G., Peng, X., Fichou, D., and Garnier, E. (1991) *J. Mol. Electron.*, **7**, 85.
18. Kelley, T.W., Muires, D.V., Paul, F.B., Smith, T.P., and Jones, T.D. (2003) *MRS Symp. Proc.*, **771**, 169–179.
19. Sheraw, C.D., Jackson, T.N., Eaton, D.L., and Anthony, J.E. (2003) *Adv. Mater. (Weinheim, Ger.)*, **15**, 2009–2011.
20. Anthony, J.E., Eaton, D.L., and Parkin, S.R. (2002) *Org. Lett.*, **4**, 15–18.
21. Payne, M.M., Parkin, S.R., Anthony, J.E., Kuo, C.C., and Jackson, T.N. (2005) *J. Am. Chem. Soc.*, **127**, 4986–4987.
22. Anthony, J.E., Brooks, J.S., Eaton, D.L., and Parkin, S.R. (2001) *J. Am. Chem. Soc.*, **123**, 9482–9483.
23. Rivnay, J., Jimison, L.H., Northrup, J.E., Toney, M.F., Noriega, R., Lu, S., Marks, T.J., Facchetti, A., and Salleo, A. (2009) *Nat. Mater.*, **8**, 952–958.
24. Subramanian, S., Park, S.K., Parkin, S.R., Podzorov, V., Jackson, T.N., and Anthony, J.E. (2008) *J. Am. Chem. Soc.*, **130**, 2706–2707.
25. Kim, Y., Cook, S., Tuladhar, S.M., Choulis, S.A., Nelson, J., Durrant, J.R., Bradley, D.D.C., Giles, M., McCulloch, I., Ha, C.-S., and Ree, M. (2006) *Nat. Mater.*, **5**, 197–203.
26. Sirringhaus, H., Brown, P.J., Friend, R.H., Nielsen, M.M., Bechgaard, K., Langeveld-Voss, B.M.W., Spiering, A.J.H., Janssen, R.A.J., Meijer, E.W., Herwig, P., and de Leeuw, D.M. (1999) *Nature*, **401**, 685–688.
27. Singh, K.A., Sauve, G., Zhang, R., Kowalewski, T., McCullough, R.D., and Porter, L.M. (2008) *Appl. Phys. Lett.*, **92**, 263303/1–263303/3.
28. Wang, C., Jimison, L.H., Goris, L., McCulloch, I., Heeney, M., Ziegler, A., and Salleo, A. (2010) *Adv. Mater.*, **22**, 697–701.
29. Chan, C.K., Richter, L.J., Dinardo, B., Jaye, C., Conrad, B.R., Ro, H.W., Germack, D.S., Fischer, D.A., De Longchamp, D.M., and Gundlach, D.J. (2010) *Appl. Phys. Lett.*, **96**, 133304/1–133304/3.
30. Baeg, K.-J., Khim, D., Kim, D.-Y., Koo, J.B., You, I.-K., Choi, W.S., and Noh, Y.-Y. (2010) *Thin Solid Films*, **518**, 4024–4029.
31. Zen, A., Pflaum, J., Hirschmann, S., Zhuang, W., Jaiser, F., Asawapirom, U., Rabe, J.P., Scherf, U., and Neher, D. (2004) *Adv. Funct. Mater.*, **14**, 757–764.
32. Babel, A. and Jenekhe, S.A. (2005) *Synth. Met.*, **148**, 169–173.
33. Zen, A., Saphiannikova, M., Neher, D., Asawapirom, U., and Scherf, U. (2005) *Chem. Mater.*, **17**, 781–786.
34. Sauve, G., Javier, A.E., Zhang, R., Liu, J., Sydlik, S.A., Kowalewski, T., and McCullough, R.D. (2010) *J. Mater. Chem.*, **20**, 3195–3201.
35. Bao, Z. and Lovinger, A.J. (1999) *Chem. Mater.*, **11**, 2607–2612.
36. Meijer, E.J., Detcheverry, C., Baesjou, P.J., van Veenendaal, E., de Leeuw, D.M., and Klapwijk, T.M. (2003) *J. Appl. Phys.*, **93**, 4831–4835.
37. McCulloch, I., Bailey, C., Giles, M., Heeney, M., Love, I., Shkunov, M., Sparrowe, D., and Tierney, S. (2005) *Chem. Mater.*, **17**, 1381–1385.
38. Abdou, M.S.A., Orfino, F.P., Son, Y., and Holdcroft, S. (1997) *J. Am. Chem. Soc.*, **119**, 4518–4524.
39. Michael, L.C., Robert, A.S., and John, E.N. (2007) *Appl. Phys. Lett.*, **90**, 123508.
40. Rost, H., Ficker, J., Alonso, J.S., Leenders, L., and McCulloch, I. (2004) *Synth. Met.*, **145**, 83–85.
41. Olsen, B.D., Jang, S.-Y., Luning, J.M., and Segalman, R.A. (2006) *Macromolecules*, **39**, 4469–4479.
42. Kline, R.J., McGehee, M.D., Kadnikova, E.N., Liu, J., and Fréchet, J.M.J. (2003) *Adv. Mater.*, **15**, 1519–1522.
43. Pokrop, R., Verilhac, J.-M., Gasior, A., Wielgus, I., Zagorska, M., Travers, J.-P., and Pron, A. (2006) *J. Mater. Chem.*, **16**, 3099–3106.
44. Verilhac, J.-M., Pokrop, R., LeBlevenec, G., Kulszewicz-Bajer, I., Buga, K., Zagorska, M., Sadki, S., and Pron, A. (2006) *J. Phys. Chem. B*, **110**, 13305–13309.
45. Jui-Fen, C., Jenny, C., Ni, Z., Henning, S., Dag, W.B., Jens, W.A., Martin, M.N., Mark, G., Martin, H., and Iain, M.

- (2006) *Phys. Rev. B (Condens. Matter Mater. Phys.)*, **74**, 115318.
46. Brinkmann, M. and Rannou, P. (2007) *Adv. Funct. Mater.*, **17**, 101–108.
 47. Urien, M., Wantz, G., Cloutet, E., Hirsch, L., Tardy, P., Vignau, L., Cramail, H., and Parneix, J.-P. (2007) *Org. Electron.*, **8**, 727–734.
 48. Kulkarni, A.P., Kong, X., and Jenekhe, S.A. (2004) *J. Phys. Chem. B*, **108**, 8689–8701.
 49. Chunyan, C., Chan, I., Volker, E., Andreas, Z., Günter, L., and Gerhard, W. (2005) *Chem. A Eur. J.*, **11**, 6833–6845.
 50. List, E.J.W., Guentner, R., de Freitas, P.S., and Scherf, U. (2002) *Adv. Mater.*, **14**, 374–378.
 51. Waltman, R.J., Bargon, J., and Diaz, A.F. (2002) *J. Phys. Chem.*, **87**, 1459–1463.
 52. Sugimoto, R.I., Takeda, S., Gu, H.B., and Yoshino, K. (1986) *Chem. Express*, **1**, 635–638.
 53. McCullough, R.D. and Lowe, R.D. (1992) *J. Chem. Soc., Chem. Commun.*, **1**, 70–72.
 54. Iraqi, A. and Barker, G.W. (1998) *J. Mater. Chem.*, **8**, 25–29.
 55. Guillerez, S. and Bidan, G. (1998) *Synth. Met.*, **93**, 123–126.
 56. Wu, X., Chen, T.-A., and Rieke, R.D. (2002) *Macromolecules*, **28**, 2101–2102.
 57. Heuze, K. and McCullough, R.D. (1999) *Polym. Prepr.*, **40**, 854.
 58. Yoon, M.H., DiBenedetto, S.A., Facchetti, A., and Marks, T.J. (2005) *J. Am. Chem. Soc.*, **127**, 1348–1349.
 59. Milian Medina, B., Van Vooren, A., Brocorens, P., Gierschner, J., Shkunov, M., Heeney, M., McCulloch, I., Lazzaroni, R., and Cornil, J. (2007) *Chem. Mater.*, **19**, 4949–4956.
 60. Heeney, M., Bailey, C., Genevicius, K., Shkunov, M., Sparrowe, D., Tierney, S., and McCulloch, I. (2005) *J. Am. Chem. Soc.*, **127**, 1078–1079.
 61. Archer, W.J. and Taylor, R. (1982) *J. Chem. Soc. Perkin Trans. 2*, 295–299.
 62. Otsubo, T., Kono, Y., Hozo, N., Miyamoto, H., Aso, Y., Ogura, F., Tanaka, T., and Sawada, M. (1993) *Bull. Chem. Soc. Jpn.*, **66**, 2033–2041.
 63. Yasuike, S., Kurita, J., and Tsuchiya, T. (1997) *Heterocycles*, **45**, 1891–1894.
 64. Heeney, M., Bailey, C., Genevicius, K., Giles, M., Shkunov, M., Sparrowe, D., Tierney, S., Zhang, W., and McCulloch, I. (2005) *Proc. SPIE-Int. Soc. Opt. Eng.*, **5940**, 594007/1.
 65. Tsao, H.N., Cho, D., Andreasen, J.W., Rouhanipour, A., Breiby, D.W., Pisula, W., and Müllen, K. (2009) *Adv. Mater.*, **21**, 209–212.
 66. McCulloch, I., Heeney, M., Chabiny, M.L., DeLongchamp, D., Kline, R.J., Cölle, M., Duffy, W., Fischer, D., Gundlach, D., Hamadani, B., Hamilton, R., Richter, L., Salleo, A., Shkunov, M., Sparrowe, D., Tierney, S., and Zhang, W. (2009) *Adv. Mater.*, **21**, 1091–1109.
 67. McCulloch, I., Heeney, M., Bailey, C., Genevicius, K., MacDonald, I., Shkunov, M., Sparrowe, D., Tierney, S., Wagner, R., Zhang, W., Chabiny, M.L., Kline, R.J., McGehee, M.D., and Toney, M.F. (2006) *Nat. Mater.*, **5**, 328–333.
 68. Anthony, J.E. (2006) *Chem. Rev.*, **106**, 5028–5048.
 69. Salleo, A., Chabiny, M.L., Yang, M.S., and Street, R.A. (2002) *Appl. Phys. Lett.*, **81**, 4383–4385.
 70. Kline, R.J., Dean, M.D., Daniel, A.F., Eric, K.L., Martin, H., Iain, M., and Michael, F.T. (2007) *Appl. Phys. Lett.*, **90**, 062117.
 71. Chabiny, M.L., Toney, M.F., Kline, R.J., McCulloch, I., and Heeney, M. (2007) *J. Am. Chem. Soc.*, **129**, 3226–3237.
 72. Hamadani, B.H., Gundlach, D.J., McCulloch, I., and Heeney, M. (2007) *Appl. Phys. Lett.*, **91**, 243512.
 73. Hawkins, D.W., Iddon, B., Longthorne, D.S., and Rosyk, P.J. (1994) *J. Chem. Soc., Perkin Trans. 1*, **19**, 2735–2743.
 74. Fuller, L.S., Iddon, B., and Smith, K.A. (1997) *J. Chem. Soc. Perkin Trans. 1*, **22**, 3465–3470.
 75. Goffri, S., Muller, C., Stingelin-Stutzmann, N., Breiby, D.W., Radano, C.P., Andreasen, J.W., Thompson, R., Janssen, R.A.J., Nielsen, M.M., Smith, P., and Siringhaus, H. (2006) *Nat. Mater.*, **5**, 950–956.
 76. Hamilton, R., Smith, J., Ogier, S., Heeney, M., Anthony, J.E., McCulloch, I., Bradley, D.D.C., Veres, J., and Anthopoulos, T.D. (2009) *Adv. Mater.*, **21**, 1166–1171.

77. Stingelin-Stutzmann, N., Smits, E., Wondergem, H., Tanase, C., Blom, P., Smith, P., and de Leeuw, D. (2005) *Nat. Mater.*, **4**, 601–606.
78. Horowitz, G. and Delannoy, P. (1991) *J. Appl. Phys.*, **70**, 469–475.
79. Meijer, E.J., Gelinck, G.H., van Veenendaal, E., Huisman, B.-H., de Leeuw, D.M., and Klapwijk, T.M. (2003) *Appl. Phys. Lett.*, **82**, 4576–4578.
80. Horowitz, G., Hajlaoui, R., Fichou, D., and Kassmi, A.E. (1999) *J. Appl. Phys.*, **85**, 3202–3206.
81. Dodabalapur, A., Torsi, L., and Katz, H.E. (1995) *Science*, **268**, 270–271.
82. Hoffman, R.L. (2004) *J. Appl. Phys.*, **95**, 5813–5819.
83. Fix, W., Ullmann, A., Ficker, J., and Clemens, W. (2002) *Appl. Phys. Lett.*, **81**, 1735–1737.
84. Fishchuk, I.I., Kadashchuk, A., Bäessler, H., and Nešpurek, S. (2003) *Phys. Rev. B*, **67**, 224303.
85. Horowitz, G., Hajlaoui, M.E., and Hajlaoui, R. (2000) *J. Appl. Phys.*, **87**, 4456–4463.
86. Podzorov, V., Menard, E., Borissov, A., Kiryukhin, V., Rogers, J.A., and Gershenson, M.E. (2004) *Phys. Rev. Lett.*, **93**, 086602.
87. Brown, A.R., Jarrett, C.P., de Leeuw, D.M., and Matters, M. (1997) *Synth. Met.*, **88**, 37–55.
88. Peisert, H., Knupfer, M., and Fink, J. (2002) *Appl. Phys. Lett.*, **81**, 2400–2402.
89. Hong, J.-P., Park, A.-Y., Lee, S., Kang, J., Shin, N., and Yoon, D.Y. (2008) *Appl. Phys. Lett.*, **92**, 143311.
90. Veres, J., Ogier, S., Leeming, S.W., Cupertino, D.C., and Khaffaf, S.M. (2003) *Adv. Funct. Mater.*, **13**, 199–204.
91. Lim, S.C., Kim, S.H., Lee, J.H., Kim, M.K., Kim, D.J., and Zyung, T. (2005) *Synth. Met.*, **148**, 75–79.
92. Klauk, H., Zschieschang, U., Pflaum, J., and Halik, M. (2007) *Nature*, **445**, 745–748.